Nanoscale Structural Engineering via Phase Segregation: Au−Ge System

Yu-Lun Chueh,[†,§,||,⊥] Cosima N. Boswell,[†,§] Chun-Wei Yuan,[†,§] Swanee J. Shin,[†,§] Kuniharu Takei,[†,§,||] Johnny C. Ho,[†,§,||] Hyunhyub Ko,[†,§,||] Zhiyong Fan,[†,§,||] E. E. Haller,[†,§] D. C. Chrzan,[†,§] and Ali Javey[†,§,||,*]

[†]Department of Electrical Engineering and Computer Sciences, University of California at Berkeley, Berkeley, California 94720, [‡]Department of Materials Science and Engineering, University of California at Berkeley, Berkeley, California 94720, [§]Materials Sciences Division, Lawrence Berkeley National Laboratory, Berkeley, California 94720, and [||]Berkeley Sensor and Actuator Center, University of California at Berkeley, Berkeley, California 94720

ABSTRACT A tunable structural engineering of nanowires based on template-assisted alloying and phase segregation processes is demonstrated. The Au−Ge system, which has a low eutectic temperature and negligible solid solubility ($<10^{-3}$ atom %) of Au in Ge at low temperatures, is utilized. Depending on the Au concentration of the initial nanowires, final structures ranging from nearly periodic nanodisk patterns to core/shell and fully alloyed nanowires are produced. The formation mechanisms are discussed in detail and characterized by in situ transmission electron microscopy and energy-dispersive spectrometry analyses. Electrical measurements illustrate the metallic and semiconducting characteristics of the fully alloyed and alternating Au/Ge nanodisk structures, respectively.

KEYWORDS Phase segregation, nanowires, nanoscale diffusion, supercooling

The ability to control the size, structure, composition, and morphology of nanowires (NWs) presents an ideal platform for elucidating nanoscale phenomena while exploring a wide range of potential technological applications.[1] In the past, researchers have demonstrated the synthesis of NW materials with tailored composition by altering the precursors during the growth process, for instance, resulting in superlattice structures with unique electrical and optical properties.[2] Here, we present a different approach, involving the postgrowth engineering of the NW structure and composition through the alloying and phase segregation of binary compounds induced by thermal annealing. As an example, we utilized the Au−Ge system which has a low eutectic temperature (361 °C) with negligible Au solid solubility ($<10^{-3}$ atom %) in Ge at room temperature.[3] In this approach, Ge/Au core/shell NWs with a HfO_2 capping layer are first prepared and then thermally annealed during which a wide range of nanostructures are controllably formed depending on the initial Au content and the annealing conditions. This approach presents a novel route for controlling the NW composition and structure with potential implications for applications in phase change memory, optoelectronic, and electronic nanodevices.

The overall concept of this structural nanoengineering process is schematically illustrated in Figure 1. Ge NWs are
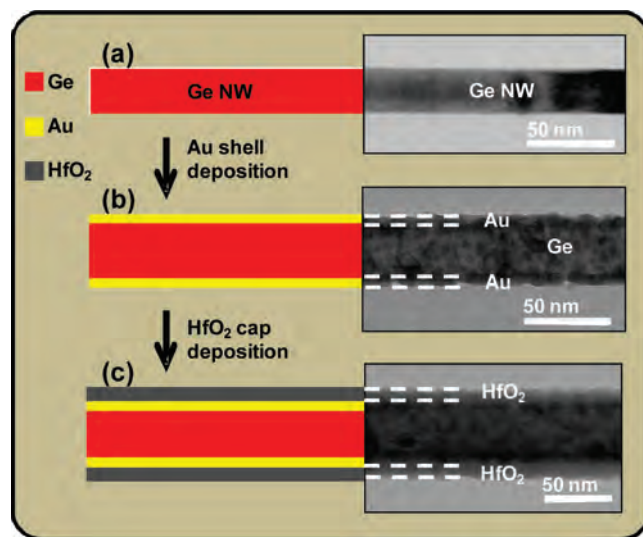
FIGURE 1. The fabrication scheme and the corresponding TEM images of the initial Ge/Au core/shell NWs with a 10 nm HfO_2 capping layer. (a) Single-crystalline Ge NWs with diameter $d = 50−60$ nm are first grown. (b) Au shell with tunable thickness is sputtered on the surface of the NWs. (c) HfO_2 capping layer is deposited on the outer surface by ALD at a sample temperature of 150 °C.

first synthesized by the vapor−liquid−solid process as previously reported elsewhere[4] with diameters $d = 50−60$ nm (Figure 1a). Next, a Au layer is sputtered on the surface of the Ge NW arrays with thickness of $t_{Au} = 2−15$ nm (Figure 1b). The thickness of the sputtered Au layer determines the overall Au:Ge atomic ratio of the NWs (see Figure S1 in Supporting Information). The NWs are then capped with ~10 nm thick HfO_2 deposited by atomic layer deposition
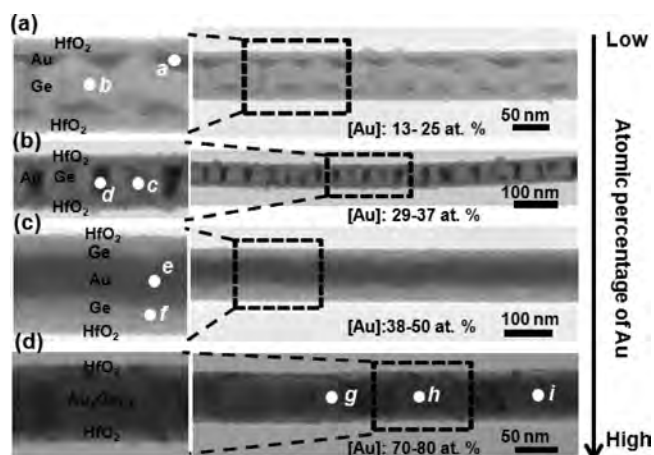
FIGURE 2. TEM images of the enabled Au/Ge nanostructures after thermal annealing at 450 °C for NWs with (a) 13−25, (b) 29−37, (c) 38−50, and (d) 70−80 atom % Au.

TABLE 1. EDS Composition Analysis of Different NW Regions As Labeled in Figure 2

position	Ge (atom %)	Au (atom %)
a	3	97
b	98	2
c	98	4
d	1	99
e	6	94
f	82	18
g	23	77
h	28	72
i	20	80

(ALD) (Figure 1c). Finally, thermal annealing at 450 °C for 5 min is performed in forming gas (95 % Ar and 5 % H₂) with heating and cooling rates of ∼7.5 and 1.5 °C/s, respectively. Notably, the 10 nm thick HfO_2 capping layer is essential for serving as a nanoscale template for the controlled formation of the Au/Ge nanostructures. Without the HfO_2 template, the overall shape and structure of NWs are uncontrollably altered during the annealing step due to the partial or full melting of the NWs at the elevated temperatures (Figure S2 in Supporting Information).

Panels a–d of Figure 2 show the representative transmission electron microscope (TEM) images of a series of Au/Ge nanostructures formed via the described process for NW samples with low to high overall Au atomic percentage, respectively. At low Au concentrations (<25 atom %), pyramid shaped, Au-rich (∼97 atom % from EDS quantitative analysis, Table 1) islands are formed on the outer surface of the NWs, beneath the HfO_2 capping layer (Figure 2a). In contrast, near periodic nanodisk patterns are formed as the Au concentration is increased to 29−37 atom % (Figure 2b). These periodic structures are composed of alternating Ge-rich (96 atom %, Table 1 and Figure S3 in Supporting Information) and Au-rich (99 atom %, Table 1) regions. As the Au concentration is further increased to 38−50 atom %, most structures exhibit Au/Ge core/shell characteristics (Fig-

ure 2c). Finally, once the Au content increases to 70−80 atom %, NWs are fully transformed to Au_xGe_{1-x} alloys (Figure 2d).

The formation of various NW structures may be understood through consideration of the phase diagram of the Au−Ge system and the eutectic solidification and/or solid state diffusion of the corresponding atoms during the cooling step. Specifically, upon heating, a volume fraction of the NWs is molten, the extent of which depends on the Au content and the annealing temperature as governed by the phase diagram.[5] During the subsequent cooling step, phase segregation and, perhaps, solid diffusion of Ge atoms take place for certain structures, resulting in the formation of Au-rich and Ge-rich patterns.

A schematic representation of the proposed formation mechanism of the Au/Ge nanostructures is shown in Figure 3. Thermal annealing of the samples with low Au concentration (<25 atom %) results in the formation of Au_xGe_{1-x} liquid droplets (Figure 3a1) with the bulk of the Ge remaining in the solid phase (melting point of bulk Ge ∼937 °C). During the cooling step, Au_xGe_{1-x} droplets are solidified and Ge atoms are segregated out of the Au_xGe_{1-x} droplets, resulting in pyramidal-shaped features that are Au-rich (Figure 3a2). For samples with 29−37 atom % Au, the resulting Au_xGe_{1-x} droplets are larger in size since a larger volume fraction of the NWs is molten during the thermal annealing step, resulting in the formation of disklike structures (Figure 3b1), a configuration that presumably minimizes, at least locally, the interfacial free energy.[6] During the cool-down step, Ge atoms segregate out of the Au_xGe_{1-x} regions, resulting in the formation of alternating Ge-rich (96 atom %) and Au-rich (99 atom %) regions (Figure 3b2). For samples with 38−50 atom % Au, Au/Ge core/shell structures were observed. By use of the TEM image in Figure 2c, the radius of the inner Au-rich core and thickness of the Ge-rich shell were measured to be $r_{Au} = 28.1$ nm and $t_{Ge} = 17.5$ nm, respectively. From this, it was calculated that the NW is composed of ∼45 atom % Au, consistent with the initial Au sputtering condition. ON the basis of the bulk phase diagram, at 450 °C, this NW consists of 57−75 vol % Au_xGe_{1-x} liquid alloy with $x ∼ 0.67$. The remaining volume is pure Ge solid. In this case, a continuous Au_xGe_{1-x} molten core is formed with a solid Ge shell (Figure 3c1). It is not immediately clear that the observed configuration represents a global free energy minimum with respect to interfacial free energy, as one might expect the Rayleigh instability to intervene.[7] However, the Rayleigh instability may be suppressed by the constraint of the outer shell and/or the observed configuration may well be a local free energy minimum. Once again, during the cool-down step, solid-state diffusion of Ge out of the Au_xGe_{1-x} core takes place, resulting in the formation of an Au-rich core and Ge-rich shell (Figure 3c2). Finally, when the Au content is increased to 70−80 atom %, which is near the eutectic point for the bulk Au−Ge system, NWs are fully molten at 450 °C, resulting in the formation of fully alloyed NWs (Figure 3d1). In this
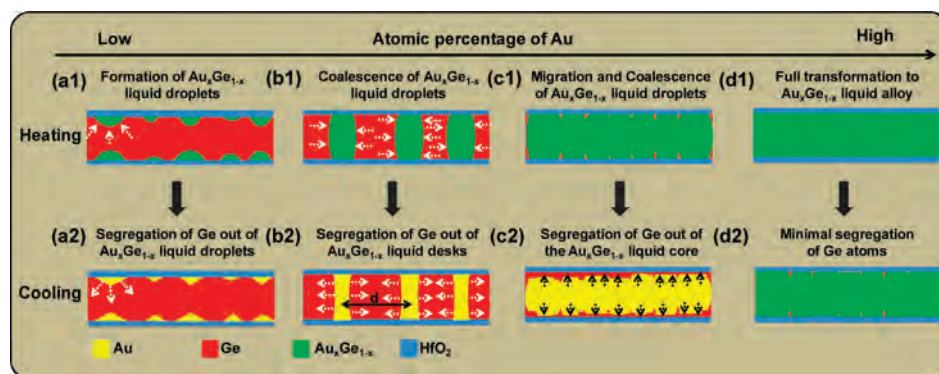
FIGURE 3. Schematic of the proposed formation mechanism for the various Au/Ge nanostructures enabled by thermal annealing process for (a) 13−25, (b) 29−37, (c) 38−50, (d) and 70−80 atom % Au.
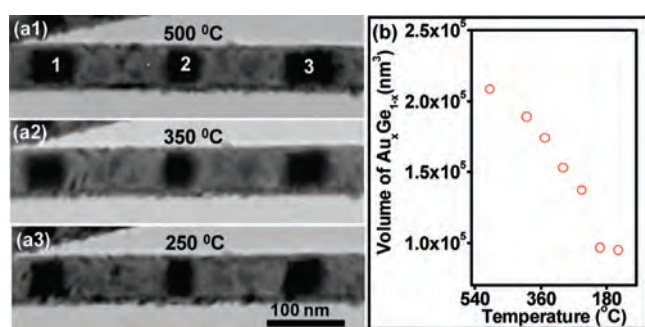

FIGURE 4. In situ TEM analysis for a NW sample with 29−37 atom % Au at (a1) 500 °C, (a2) 350 °C, and (A3) 250 °C. The TEM images correspond to the cool-down step. (b) The total volume of regions 1, 2, and 3 (as labeled in (a1)) as a function of temperature.

case, minimal phase segregation and solid-state diffusion of Ge from the alloy are observed during the cool-down step presumably due to the lack of solid Ge nucleation sites to facilitate the process (Figure 3d2). Apparently, the cooling rate is fast enough and the solidification temperature is low enough such that the structure is kinetically limited to remain alloyed.

To further investigate the segregation behavior during the cool-down step, in situ TEM studies of NW samples with 29−37 atom % Au were conducted. In this case, the total volume of regions 1, 2, and 3 (Au_xGe_{1-x} nanodisk regions) in Figure 4a1 at different temperatures was measured, summed, and plotted, as shown in Figure 4b. The total volume of the disk patterns decreased by a factor of ∼2 as the temperature was reduced from 500 to ∼200 °C, beyond which minimal volume change is observed. Notably, the phase diagram governing our NWs appears near that of the bulk eutectic alloy as determined from the temperature dependency of the volume of Au_xGe_{1-x} droplets (Figure S5 in Supporting Information).

The volume vs temperature curve varies smoothly between 500 and 200 °C suggesting that the eutectic liquid may be supercooled, as has been observed in free-standing Au−Ge alloys.[5] The strong segregation likely occurs upon solidification of the supercooled liquid eutectic alloy. We note that the solid-state diffusion of Ge atoms out of the

Au_xGe_{1-x} regions may also account for the observed segregation. In either case, the result is the formation of crystalline, lens-shaped regions of nearly pure Au (Figures S3 and S4 in Supporting Information). At lower temperatures (<200 °C), the diffusion of Ge atoms is minimal with the Au_xGe_{1-x} volume remaining constant (Figure 4b). This result provides strong support for the proposed mechanism of the Au/Ge nanostructure formation, involving first the formation of liquid Au_xGe_{1-x} alloys at elevated temperatures, followed by the segregation of Ge out of the alloy during the cool down step. Furthermore, the in situ TEM analyses confirm that the alloyed droplets remain in their original positions up to a temperature of 500 °C, even when the annealing time is 1 h, and also during the cooling process (Figure 4a2 and Figure 4a3).

The nanodisk patterns are not likely to be the equilibrium ground state, but they may be unusually long-lived metastable states. Consideration of the chemical potential of Au atoms within two adjacent disks suggests that the disk coarsening kinetics may be sluggish.[8] In the simplest analysis, the transfer of a Au atom from one disk to the other does not alter the free energy of the system: the total interface energy is unaltered by this transfer. If, however, two disks "touch", they can relax to eliminate two disk surfaces. This, of course, provides a driving force for coarsening. However, the coarsening mechanism requires the motion of the center of mass of the disks, and this occurs only through the emission and adsorption of atoms by the disks. As the distance between disks increases, the time between disk collisions increases, eventually resulting in the observed nanodisk patterns with semiperiodic separations of 50−100 nm (Figure 2b and Figure 4a).

To investigate the properties of the Au/Ge nanostructures, electrical transport measurements were conducted for two different systems: (i) nearly periodic Au/Ge nanodisk and (ii) Au_xGe_{1-x} alloyed NWs. For device fabrication, thermally annealed NWs were harvested from the growth substrate and drop-cast on a Si/Si_3N_4 (100 nm) substrate. Photolithography of a positive photoresist layer was performed to define source/drain (S/D) patterns followed by reactive ion etching
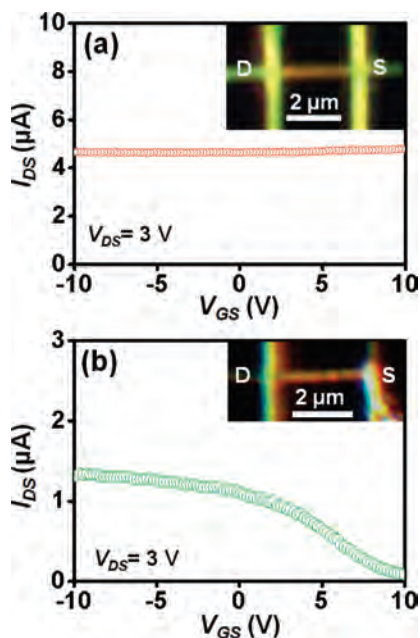
FIGURE 5. Electrical measurements of back-gated devices based on (a) fully alloyed Au$_x$Ge$_{1-x}$ NW and (b) periodic Au/Ge nanodisk NW, showing metallic and semiconducting behaviors, respectively. The insets show the corresponding dark field optical images of the NW devices.

to remove the HfO$_2$[9] outer shell of the NWs in the patterned regions. Subsequently, Ni (~50 nm thick) was thermally evaporated followed by the photoresist lift-off, resulting in the formation of Ni S/D electrodes. The heavily doped Si substrate was used as the global back-gate with a Si$_3$N$_4$ gate dielectric. Parts a and b of Figure 5 show the source/drain current (I_{DS}) as a function of the back-gate voltage (V_{GS}) for the Au$_x$Ge$_{1-x}$ alloyed NW and the periodic Au/Ge disk NWs, respectively. The corresponding dark field optical images for both structures are shown in the insets of parts a and b of Figure 5. Notably, the periodic Au/Ge nanodisk patterns are clearly evident from the dark-field optical microscopy (Figure 5b) due to the difference in the light scattering between the two regions while no optical contrast along the NW length is observed for the fully alloyed system (Figure 5a). The fully alloyed Au$_x$Ge$_{1-x}$ NWs exhibit a near metallic behavior without significant gate dependence in the drain current (Figure 5a). A resistivity of ~2.1 mΩ·cm can be calculated by taking length and radius of ~2.8 μm and ~30 nm, respectively, which is consistent with the bulk Au$_x$Ge$_{1-x}$ resistivity values of 5–10 mΩ·cm previously reported in the literature.[10] On the other hand, the periodic nanodisk NWs exhibit a p-type semiconducting behavior arising from the nearly pure Ge islands along the length of the NWs. In this structure, holes are transported along the length of the NWs by sequential injection between the Au-rich and Ge-rich disks. The p-type characteristic may arise from the Schottky barrier heights associated with the system with a lower barrier height for holes as compared to the electrons. Ad-

ditionally, surface states[11] may induce Fermi-level pinning that could also contribute to the observed characteristics.

While in the current study, equilibrium heating and cooling processes were utilized with relatively long time scales; in the future, ultrafast, nonequilibrium processes may be applied to further characterize the proposed system and to enable the formation of other types of nanostructures. This concept of structural engineering via phase segregation by modifying the atomic percentage ratios of the metal layer may also be applicable to other systems with negligible solid solubility limits such as SnGe and AgGe.[12] Additionally, in the future, detailed theoretical calculations of the relevant energies and the nanoscale phase diagram of the system are needed to further shed light on the kinetics of the proposed structural nanoengineering process.

In summary, a new concept for tailoring the composition and structure of NWs via alloying and phase segregation is demonstrated based on the Au–Ge system. Four distinct morphological structures, including island-like, periodic nanodisks, core/shell, and fully Au$_x$Ge$_{1-x}$ alloyed NWs, were enabled by controlling the atomic percentage of Au and thermal annealing above the eutectic temperature. The formation mechanism of the structures is discussed and characterized by in situ TEM. The electric measurements illustrate metallic and semiconductor behavior for the fully alloyed and nanodisk patterned NWs, respectively, demonstrating the ability to control the NW properties by tailoring the structure.

Supporting Information Available. Schematic figures on how to calculate the Au atomic percentage, of the TEM images of Ge NWs coated with Au but without a HfO$_2$ cap before and after annealing, and of EDS line profiles for nanodisk and Au$_x$Ge$_{1-x}$ alloyed NWs, and a figure demonstrating the behavior of the nanodisk patterns based on the bulk and nanoscale phase diagrams. These materials are available free of charge via the Internet at http://pubs.acs.org.

REFERENCES AND NOTES
(1)   (a) Lieber, C. M. *MRS Bull.* **2003**, *28*, 486. (b) Javey, A. *ACS Nano* **2008**, *2*, 1329. (c) Wang, Z. L. *Mater. Today* **2004**, *7* (6), 26. (d) Yang, P. *MRS Bull.* **2005**, *30*, 85. (e) Wang, Z. L. *J. Mater. Chem.* **2005**, *15*, 1021. (f) Fan, Z.; Razavi, H.; Do, J.; Moriwaki, A.; Ergen, O.; Chueh, Y.-L.; Leu, P. W.; Ho, J. C.; Takahashi, T.; Reichertz, L. A.; Neale, S.; Yu, K.; Wu, M.; Ager, J. W.; Javey, A. *Nat. Mater.* **2009**, *8*, 648. (g) Ho, J. C.; Yerushalmi, R.; Jacobson, Z. A.; Fan, Z.; Alley, R. L.; Javey, A. *Nat. Mater.* **2008**, *7*, 62.
(2)   (a) Gudiksen, M. S.; Lauhon, L. J.; Wang, J.; Smith, D. C.; Lieber, C. M. *Nature* **2002**, *415*, 617. (b) Bjork, M. T.; Ohlosson, B. J.; Sass,

T.; Persson, A. I.; Thelander, C.; Magnusson, M. H.; Deppert, K.; Wallenberg, L. R.; Samuelson, L. *Nano Lett.* **2002**, *2*, 87. (c) Bjork, M. T.; Ohlosson, B. J.; Sass, T.; Persson, A. I.; Thelander, C.; Magnusson, M. H.; Deppert, K.; Wallenberg, L. R.; Samuelson, L. *Nano Lett.* **2002**, *2*, 87.

(3) Nath, V. D.; Vankar, V. D.; Choper, K. L. *Phys. Status Solidi* **1978**, *49*, 379.

(4) Wang, D.; Tu, R.; Zhang, L.; Dai, H. *Angew. Chem., Int. Ed.* **2005**, *44*, 2.

(5) Sutter, E.; Sutter, P. *Nano Lett.* **2008**, *8*, 411.

(6) Yuan, C. W.; Shin, S. J.; Liao, C. Y.; Guzman, J.; Stone, P. R.; Watanabe, M.; Ager, J. W.; Haller, E. E.; Chrzan, D. C. *Appl. Phys. Lett.* **2008**, *93*, 193114.

(7) Wang, N.; Cai, Y.; Zhang, R. Q. *Mater. Sci. Eng. R* **2008**, *60*, 1.

(8) Boswell, C. N.; Yuan, C.-W.; Chrzan, D. C. Unpublished.

(9) For the reactive ion etching of the HfO_2 capping layer, BCl_3 (50 sccm), N_2 (50 sccm), and Cl_2 (30 sccm) gases were used at a pressure of 250 mTorr and power of 250 W. To minimize resist heating, pulsed etching cycles consisting of 10 s of plasma being on and 30 s of plasma being off were used. The total etch time was 60 s (6 cycles).

(10) (a) Sahlng, S.; Béthoux, O.; Lasjaunias, J. C.; Brusetti, R. *Phys. B* **1996**, *219&200*, 754. (b) Fortune, N. A.; Graf, M. J.; Murata, K. *Rev. Sci. Instrum.* **1998**, *69*, 133.

(11) Wang, D.; Chang, Y.-L.; Wang, Q.; Cao, J.; Farmer, D. B.; Gordon, R. G.; Dai, H. *J. Am. Chem. Soc.* **2004**, *126*, 11602.

(12) Bauer, M.; Taraci, J.; Tolle, J.; Chizmeshya, A. V. G.; Zollner, S.; Smith, D. J.; Menendez, J.; Hu, Changwu; Kouvetakis, J. *Appl. Phys. Lett.* **2002**, *81*, 2992.

Supporting Information

Nanoscale Structural Engineering via Phase Segregation: Au-Ge System

Yu-Lun Chueh,[†,∥,⊦] Cosima N. Boswell,[‡,∥] Chun-Wei Yuan,[‡,∥] Swanee J. Shin,[‡,∥] Kuniharu Takei,[†,∥,⊦] Johnny C. Ho,[†,∥,⊦] Hyunhyub Ko,[†,∥,⊦] Zhiyong Fan,[†,∥,⊦] E. E. Haller,[‡,∥] D. C. Chrzan,[‡,∥] Ali Javey[†,∥,⊦*]

[†]Department of Electrical Engineering and Computer Sciences, University of California at Berkeley, Berkeley, CA, 94720, USA.

[‡]Department of Materials Science and Engineering, University of California at Berkeley, Berkeley, CA. 94720, USA,

[∥]Materials Sciences Division, Lawrence Berkeley National Laboratory, Berkeley, CA 94720, USA.

[⊦] Berkeley Sensor and Actuator Center, University of California at Berkeley, Berkeley, CA, 94720, USA.

* Corresponding author: ajavey@eecs.berkeley.edu

Calculation of Au volume and atomic percentage

The Au concentration of the *as-made* Ge/Au core/shell NWs is estimated from equation 1.

Volume ratio [Au] = $[(r_{Au}+r_{Ge})^2-r_{Ge}^2]/(r_{Au}+r_{Ge})^2$ **Eq. 1**

where r_{Au} and r_{Ge} represent the radius of Ge core and the thickness of the Au shell, respectively as measured by TEM. Subsequently, the atomic percentage can be calculated by taking the density and atomic number of Au and Ge as flows:

$$\text{Atomic ratio of Au} = \frac{([Au]\times\frac{19.3}{79})}{\left([Au]\times\frac{19.3}{79}\right)+\left((1-[Au])\times\frac{5.3}{32}\right)}$$ **Eq. 2**

where [Au] represents the volume ratio of Au from equation 1. The solid density of Au and Ge are 19.3 g/cm^3 and 5.3 g/cm^3, respectively while the atomic numbers of Au and Ge are 79 and 32, respectively.
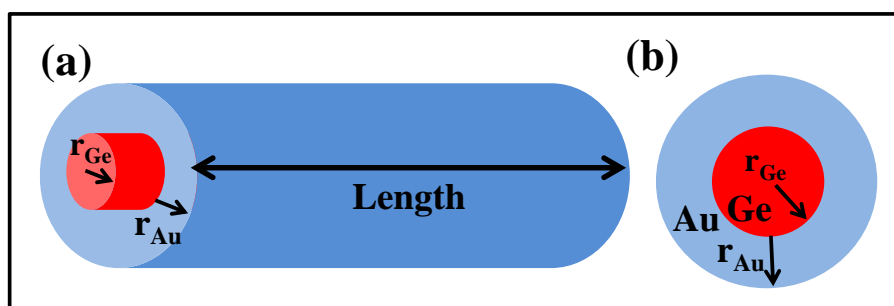

Figure S1. (a)-(b) Schematic illustration of the as-made Ge/Au core/shell NW, prior to the deposition of the HfO$_2$ capping layer.
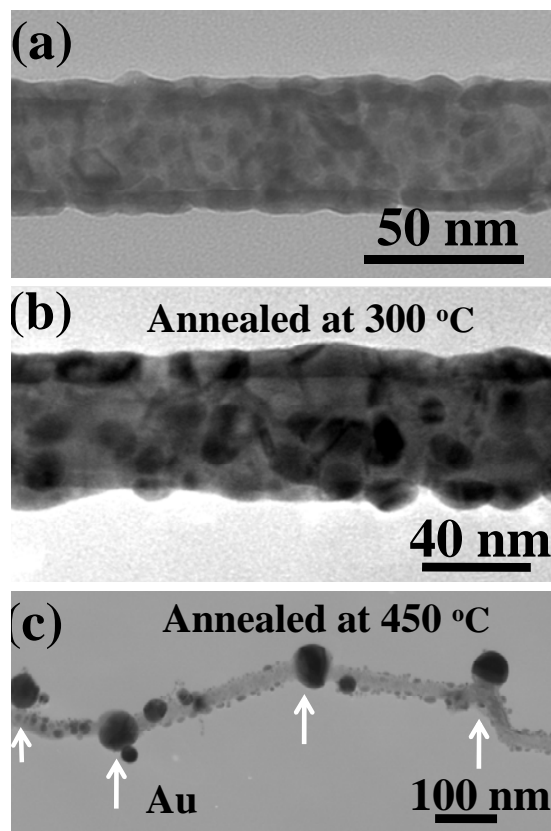
Figure S2. TEM images of Ge/Au core/shell NWs without the HfO_2 capping layer (a) before and after annealing at (b) 300 ℃ and (c) 450 ℃. Clearly, without the HfO_2 template, the NW structure and morphology are uncontrollably altered when annealed above the eutectic temperature of the Au:Ge system due to the partial or full melting of the NW.
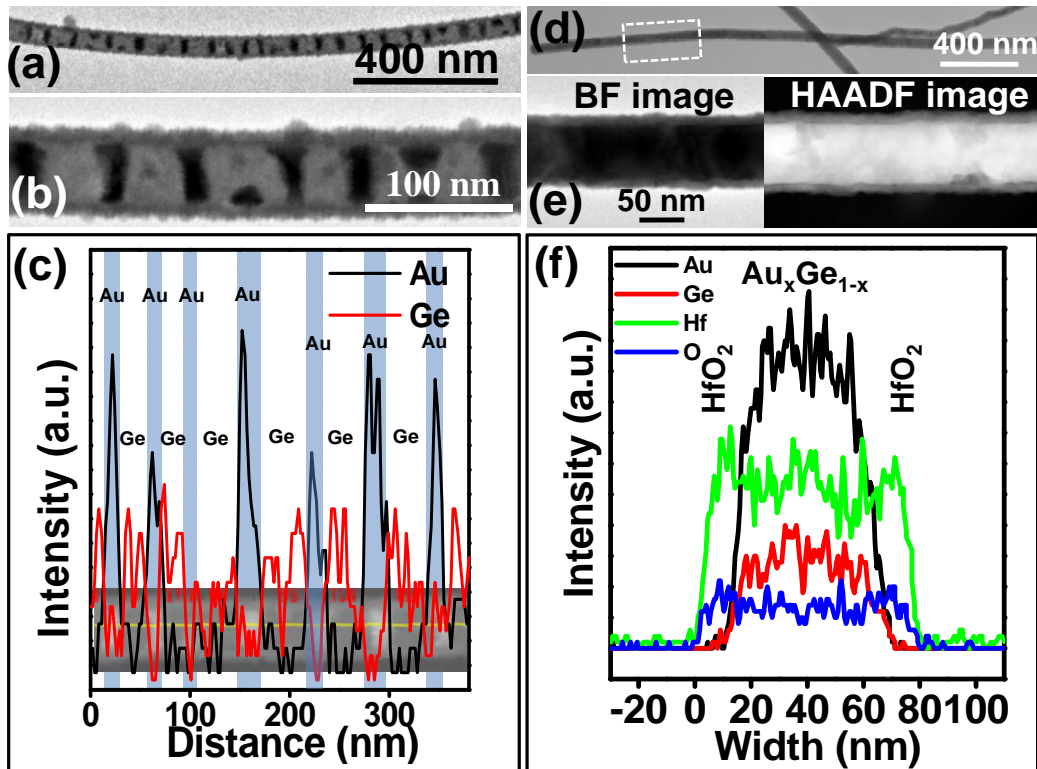
Figure S3. (a)-(b) The low and high magnification TEM images of Au/Ge periodic nanodisk structures, respectively. (c) The EDS line scan clearly shows the alternating Au-rich and Ge-rich regions. (d)-(e) The low and high magnification of a Au_xGe_{1-x} fully alloyed NW, respectively. The HAADF image highlights the fully alloyed NW composition, without noticeable phase segregation. (f) The EDS line scan of a fully alloyed NW.
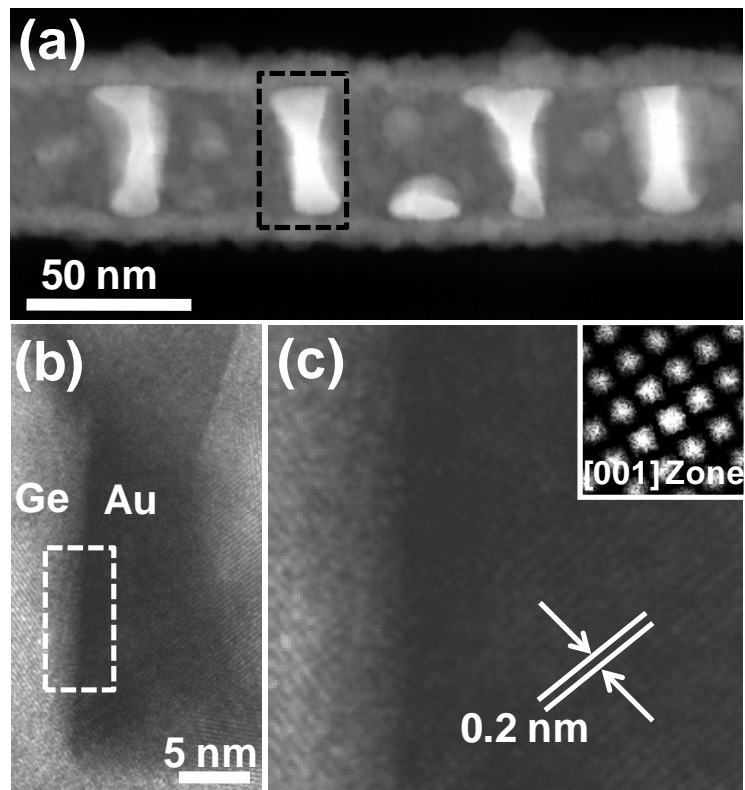
Figure S4. (a) The high angle angular dark field (HAADF) image, and (b) the corresponding

HRTEM image of Au/Ge periodic nanodisks, highlighting their crystalline structure.
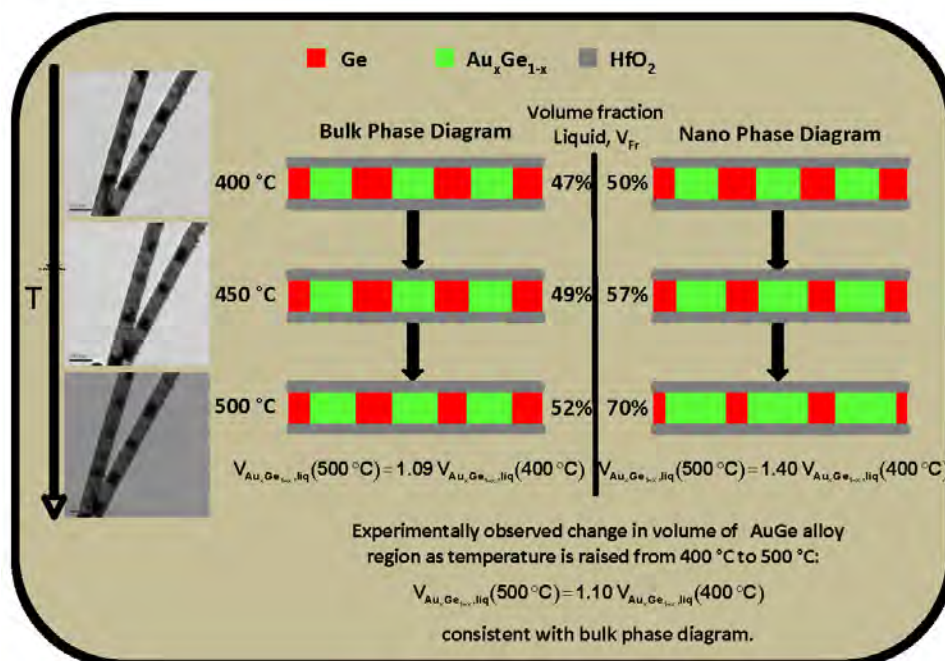
Figure S5. Using the liquidus line on the Ge rich side of the phase diagram, and assuming that the density of the Au_xGe_{1-x} liquid is the concentration weighted average of the elemental liquid densities at the elemental melting points, one can compute the expected volume of liquid at each temperature. The diagram on the left shows the predictions arising from the bulk phase diagram.[1] The predicted increase in volume from 400 °C to 500 °C is 9%. In contrast, the phase diagram of Sutter and Sutter[2] suggests an increase in volume of 40%. The experimental observation, a 10% increase in volume over the temperature range, is in good agreement with the bulk phase diagram. We conclude, therefore, that the bulk phase diagram is a better representation of our experiments. We do note, however, that our NWs have an average curvature roughly ½ of the structures considered in [2] and furthermore, our NWs are confined by the HfO_2 layer. We would expect the coating to influence the phase diagram as well.[3] However, based on the present analysis, the influence of the HfO_2 on the phase equilibria seems inconsequential.

References:

1. Okamoto, H., *Reevaluation of Thermodynamic Models for Phase Diagram Evaluation*, Journal of Phase Equilibria, **12**, 623 (1991).

2. Sutter, E. and P. Sutter, *Phase diagram of nanoscale alloy particles used for vapor-liquid-solid growth of semiconductor nanowires*, Nano Letters, **8**, 411 (2008).

3. Xu, Q., I.D. Sharp, C.W. Yuan, D.O. Yi, C.Y. Liao, A.M. Glaeser, A.M. Minor, J.W. Beeman, M.C. Ridgway, P. Kluth, J.W. Ager, D.C. Chrzan, and E.E. Haller, *Large melting-point hysteresis of Ge nanocrystals embedded in SiO2 (vol 97, art no 155701, 2006)*, Physical Review Letters, **97**, 209902 (2006).